Infectious Disease Imaging

16

Ishita Desai and Kara-Lee Pool

Introduction

The topic of infectious disease imaging in low- and middle-income countries (LMICs) is vast, and this chapter is not intended to serve as a comprehensive reference. For that, we kindly direct the reader to the remarkable text on the topic entitled *The Imaging of Tropical Diseases*, authored by the distinguished Drs. Palmer and Reeder; their comprehensive work is truly a masterpiece on the subject of infectious disease imaging in LMIC settings and includes clinical cases in multiple modalities and exhaustive reviews on pathophysiology and medical management, all of which are based on meticulous epidemiology and pathophysiology discussions [1]. In contrast, what follows in this chapter is an introductory review of the available imaging modalities followed by the imaging presentations of common endemic infectious disease processes organized by disease processes in order to highlight the continued importance imaging plays in the diagnosis and treatment of infectious diseases in an ever-evolving world.

I. Desai
Department of Radiology, UCLA,
Los Angeles, CA, USA
e-mail: idesai@mednet.ucla.edu

K.-L. Pool (✉)
Department of Radiology, UCLA,
Santa Monica, CA, USA
e-mail: kpool@mednet.ucla.edu

D. J. Mollura et al. (eds.), *Radiology in Global Health*,
https://doi.org/10.1007/978-3-319-98485-8_16

Background

Infectious diseases continue to remain a major cause of morbidity and mortality in the world [2]. The use of diagnostic imaging has increased dramatically over the past several decades, with a particularly sharp rise in advanced cross-sectional imaging systems such as computed tomography (CT), magnetic resonance imaging (MRI), and molecular imaging such as positron emission tomography (PET) and single-photon emission computed tomography (SPECT) which are expected to continue to grow [3]. However, there are significant disparities in the availability of imaging services across the globe, as discussed elsewhere in this text, and most advanced imaging is generally available only to the higher economic strata in LMICs [4]. For example, as a result of strengthening emerging economies, imaging services are growing rapidly in Brazil, Russia, India, and China (also known as BRIC countries) [5–8]. The availability and relative cost of the various imaging modalities are shown in Fig. 16.1.

Imaging Modalities

There are a great number of options available to the modern, fully equipped hospital for the diagnosis and elucidation of a large number of diseases. These options range from those that are

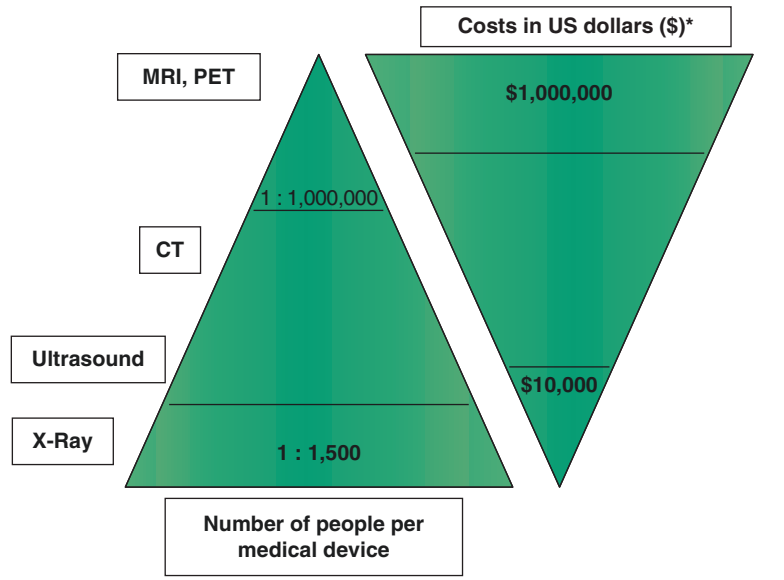

Fig. 16.1 Graphical representation illustrating the availability of the imaging modality (number of people per device) versus the cost of purchasing the imaging scanner (in US dollars) [9]. (Reprinted from Lungren et al. [9], with permission from SpringerNature)

highly complicated and time-intensive, such as MRI, to those that are simple but effective, such as ultrasound or radiography. Though this chapter is by no means an exhaustive atlas of the various uses and misuses of these imaging modalities, a small description of them is provided in order to better understand their role in global health.

MRI, the newest and perhaps least readily accessible of these modalities, was utilized in vivo in the first human in 1977 [10]. Since then, it has rapidly developed into one of the most widespread medical imaging techniques [11]. Because MRI uses a controlled magnetic field, some of the primary advantages are the lack of ionizing radiation, high spatial resolution, and excellent soft-tissue contrast. One of the main downsides to the use of MRI is the cost. Capital equipment, maintenance, and infrastructure costs alone exceed millions of dollars (US), while the technical skillset and high level of training needed to successfully acquire and interpret the images remain exceedingly difficult to obtain in low-resource countries. Though not as widely available in LMICs as other imaging technologies, emerging markets such as China are rapidly increasing the number of MRI scanners available to the local population (300–400 units per year) [12]. This is because of the increasing importance of MRI in many prior elusive diagnoses. MRI has become an exceedingly important diagnostic modality for the evaluation of the central nervous and musculoskeletal systems due to its great sensitivity [13].

CT imaging, on the other hand, has been around for decades and is more widely available. It is extensively utilized for evaluating disease processes in nearly every part of the body. Compared to standard radiography techniques, CT imaging provides three-dimensional images with excellent spatial resolution. It is relatively rapid, making it invaluable, especially in emergent or life-threatening situations [14]. However, as discussed elsewhere in this text, CT scanning, though relatively inexpensive when compared to other major advanced imaging modalities such as MRI, remains an infrastructure-intensive modality that continues to be out of reach for a majority of the world's population.

Despite the advent of advanced imaging modalities, it should be noted that plain film radiography and ultrasound continue to be mainstays in the field of imaging in low-resource areas. Radiography especially remains an important diagnostic tool for assessing pulmonary infections, but it should be noted that radiography has a limited scope in the evaluation of

intraabdominal infections. Although radiographs are quite adept at picking up many of the secondary signs of infection, including bowel obstruction, ileus, pneumatosis (air in the bowel wall), or free intraperitoneal air, they have difficulty in assessing for actual signs of inflammation [15]. Many of these secondary signs would indicate that the disease has already progressed. The usefulness of radiography is increased somewhat by the ability to administer oral contrast agents (such as barium sulfate) for improved evaluation of the gastrointestinal tract. There are, of course, cost- and availability-related drawbacks to this type of examination. For this reason, ultrasound remains an incredibly powerful diagnostic modality in and out of low-resource areas, most notably in the diagnosis and management of abdominal and pelvic infections [15], in addition to soft-tissue and thoracic infections [16, 17].

Outside low-resource areas, point-of-care ultrasound has helped expedite diagnosis and treatment. In low-resource areas, however, it is often the only available diagnostic modality [18, 19]. Several studies have demonstrated the use of ultrasound as an irreplaceable tool, affecting diagnosis and altering clinical management [20–22] in not only infectious disease but also obstetrics and cardiology.

Incredibly, there are well-defined ultrasound presentations of a multitude of tropical infections, which can help narrow down differential considerations and lead to quicker treatment. These include but are not limited to paragonimiasis, clonorchiasis, and schistosomiasis [23]. The list is growing and presents an excellent argument for the increased use and study of ultrasound in global health.

On another end, we will not extensively discuss molecular imaging, PET, and SPECT, in this chapter due primarily to its limited availability in low-resource areas and relatively limited use because of the cost, need for trained personnel, and lack of networks for synthesizing, handling, and delivering the radioactive radiotracers. These imaging modalities are currently better developed for cancer and neurology [24, 25]. There are uses for SPECT imaging to identify the site of infection, diagnose types of infection, or locate a source of infection [26, 27]. In addition, there is active research on the utility of PET/CT in the evaluation of subclinical, active pulmonary tuberculosis in HIV-1-infected adults [28]. Though these current techniques are useful in anatomically localizing the infectious lesions, they are limited by being nonspecific; these techniques cannot fully differentiate true infections from sterile inflammation or cancer.

Pneumonia

Worldwide, pneumonia is a leading cause of death and hospitalization, particularly among children and the elderly [29]. The diagnosis of pneumonia remains one of the most common applications of radiographic imaging. A simple chest radiograph can aid in the identification of the involved pathogen, guiding treatment and identifying complications and/or treatment response. Further evaluation with CT is useful, but not necessary for the diagnosis of pneumonia, particularly if resources are limited.

For example, lobar consolidation, cavitation, and effusions suggest bacterial etiology (Fig. 16.2). Of note, however, in the proper clinical setting, these findings may also indicate polymicrobial (i.e., multiple pathogens at once), fungal, or mycobacterial etiologies [30]. Diffuse bilateral involvement can be an indication of an atypical infection, such as *Mycoplasma*, *Pneumocystis jirovecii*, *Legionella*, or a primary viral illness [30]. A chest radiographic appearance more severe than suggested by the clinical examination has been described in both viral and mycoplasma pneumonias [30]. As evident, specific pathogenic diagnosis is often not possible with radiography alone, but the role of imaging in pneumonia is not to provide a specific diagnosis but rather help: (1) localize the site of infection at diagnosis, (2) monitor progression versus regression, (3) estimate severity, and (4) diagnose complications such as pneumothorax, pleural effusions, empyemas, abscesses, and atelectasis. For this reason, radiography is a vital tool for managing lung infections even when the specific pathogen is not identified, particularly since

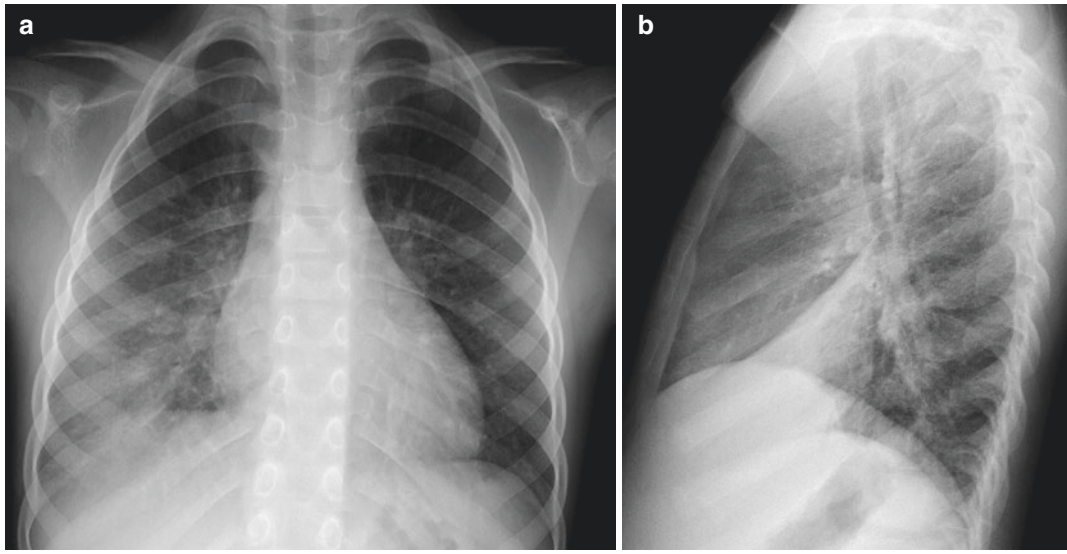

Fig. 16.2 Frontal (**a**) and lateral (**b**) chest radiograph demonstrating right lower lobe pneumonia in a 6-year-old male presenting with cough and fever

many antibiotic therapies can cover a wide range of the possible pathogens.

Empyema is the term used to describe an infected fluid collection in the pleural space. This can occur primarily but most commonly is attributable to a complication of pneumonia, previous surgery, or trauma [31]. The chest radiograph will classically demonstrate a large, lentiform (lens-shaped) pleural opacification [32] (Fig. 16.3). Pulmonary abscess, in contrast to an empyema, is an infected collection in the lung parenchyma and is often a complication of suppurative pneumonia that destroys lung parenchyma. The result is a pus-filled cavity, often demonstrating an air-fluid level on chest radiographs (Fig. 16.4) [33]. In contrast to empyemas and abscesses, necrotizing pneumonia describes the necrosis of infected pulmonary parenchyma with or without cavitation [34].

Symmetric perihilar ground-glass opacities, often termed "bat wing opacities," are frequently seen in the early stages of *Pneumocystis jirovecii* pneumonia (PCP), most often seen in HIV-infected patients [35]. In more advanced stages, PCP presents with diffuse ground-glass opacities and alveolar consolidation [35, 36]. Other less common patterns have been reported, including lobar infiltrates, pulmonary nodules, pneumatoceles, and other cystic changes [36]. These diverse features of PCP are important to recognize in imaging because this is a common opportunistic infection in HIV-infected patients and the treatment is different and longer term than the therapies for other lung infections.

Tuberculosis

Of all the infectious diseases, *Mycobacterium tuberculosis* deserves special mention due to the widespread nature of the infection, communicability, increasing resistance to treatment, and its long-term morbidity/mortality. According to the World Health Organization, new tuberculosis infections occur in about 1% of the population each year [37]. According to the 2016 WHO report on tuberculosis (TB), there were an estimated 10.4 million new cases (incident) of active TB and 1.4 million deaths, mostly occurring in LMICs [37]. There has been an effort to decelerate this incidence rate, but success in TB control also depends on the number of these cases that result in death. In Africa, for example, the case fatality ratio continues to range from 5% to 20%. In this case, imaging is invaluable to prevent progression and reduce the number of TB-related deaths [37].

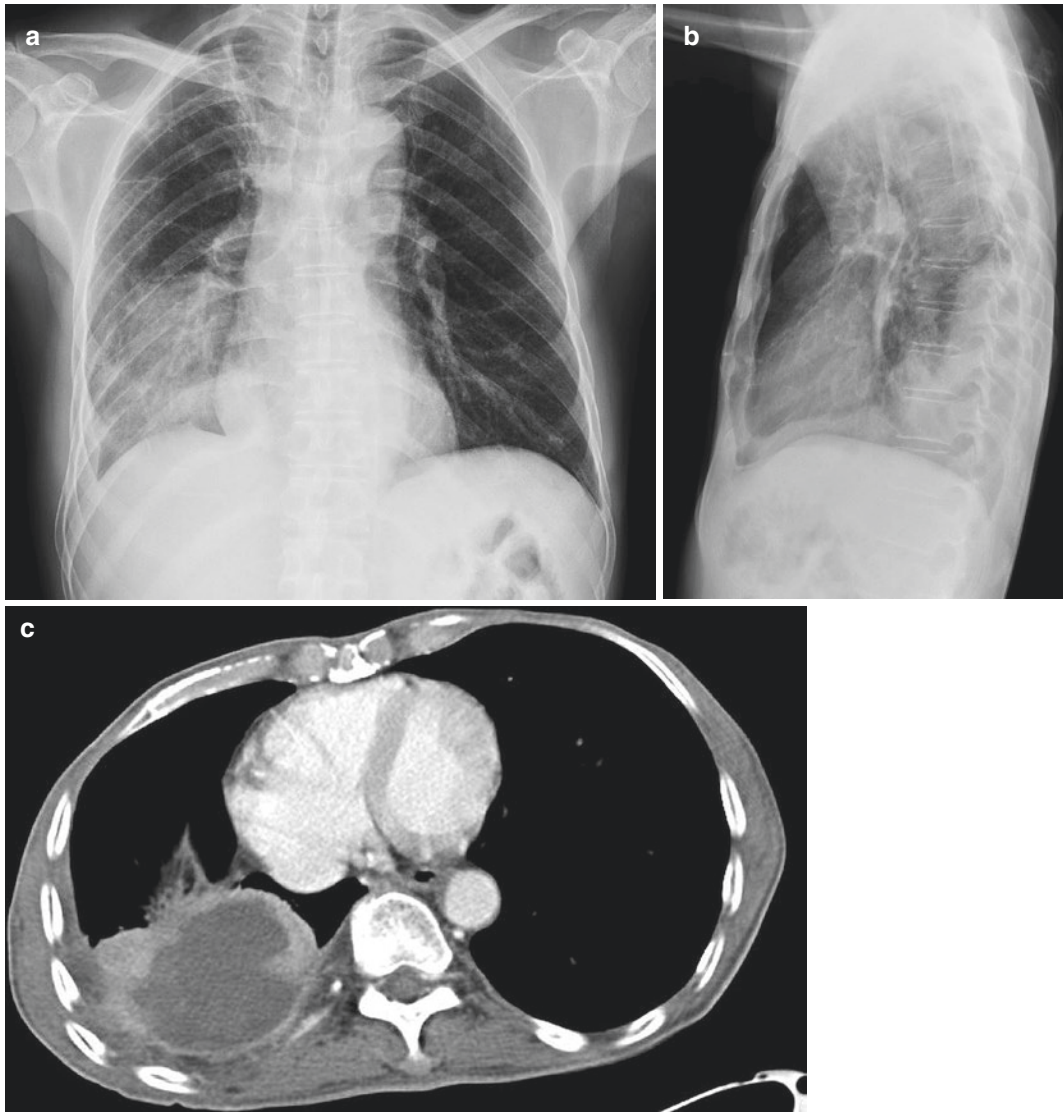

Fig. 16.3 Frontal (**a**) and lateral (**b**) chest radiographs and axial chest CT (**c**) of a 57-year-old male with a history of disseminated TB found to have an empyema, demonstrated by the lens-shaped opacity at the right lung base on the frontal radiograph, confirmed by CT

An important consideration in addressing TB prevalence and incidence is disease communicability. TB is transmitted through air by breathing in airborne particles that are generated when an infected individual coughs, sneezes, shouts, or even sings. The probability of transmission is dependent on several factors, including the concentration of infectious particles, air circulation, frequency of exposure, and physical proximity among a number of other considerations [38].

Diagnosis of active TB relies on imaging, as well as microbiological culture of body fluids, susceptibility testing, and/or nucleic acid amplification tests like GeneXpert MTB/RIF, while the diagnosis of *latent* TB relies on the tuberculin skin test (TST) and/or blood tests. Unfortunately, the acid-fast bacilli are found in the sputum in a limited number of patients with active pulmonary TB. Newer tests like GeneXpert are more rapid than mycobacterial culture and identify both the

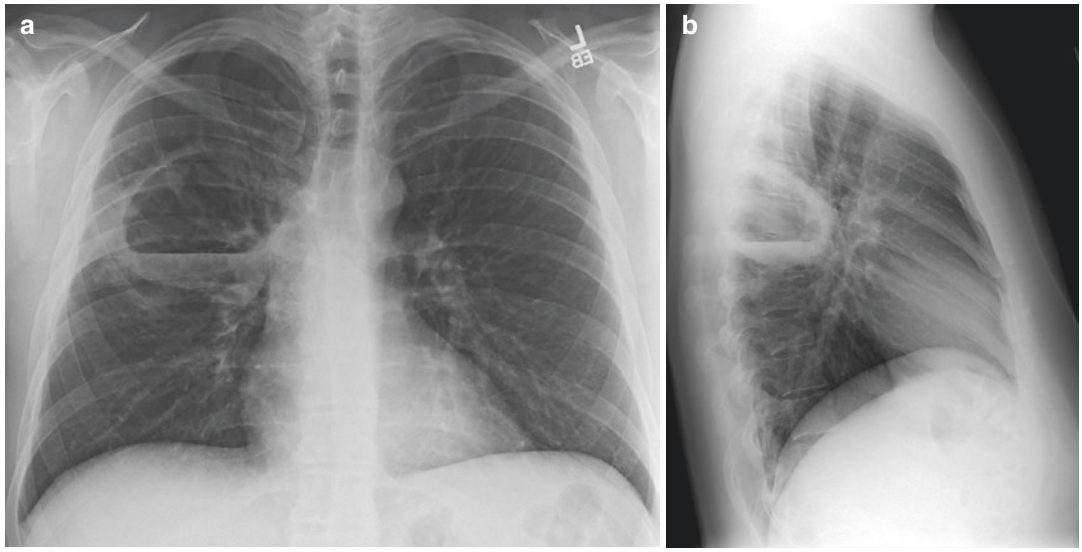

Fig. 16.4 Frontal (**a**) and lateral (**b**) chest radiographs of a 28-year-old male with a 1-month history of cough found to have a pulmonary abscess, demonstrated by a localized, walled cavity, with an air-fluid level in the right lower lobe

presence of *M. tuberculosis* and resistance to rifampin in a single test [39]. Imaging, however, still plays an important role in triaging patients, in aiding diagnosis when bacteriology cannot be confirmed, and in determining the extent of disease or complications of pulmonary TB [40].

There is also a growing role for ultrasound in the diagnosis of extrapulmonary TB. There are numerous studies that examine and enumerate the ultrasound presentation of extrapulmonary TB in the setting of HIV. The protocol for this rapid diagnosis is better known as FASH, or the focused assessment with sonography for HIV-associated TB, and has been used and tested repeatedly in resource-poor settings where CT and the described diagnostic lab tests are not easily available [20, 21, 41]. Oftentimes, the imaging provides rapid diagnosis for appropriate therapy before the definitive diagnosis by bacteriology. It is thought that more than 50% of infected patients remain undiagnosed, and lack of access to medical care, particularly medical imaging such as chest radiography, presents a significant barrier to diagnosis and disease monitoring [42]. Treatment is difficult and requires administration of multiple antibiotics, many of which are expensive, over a long period of time (i.e., greater than 6 months). Unsurprisingly, antibiotic resistance is a growing problem in multi-drug resistant TB (MDR-TB) infections.

TB can have a wide variety of radiographic appearances and thus has been termed "the great imitator." There are three classic appearances of pulmonary TB on chest radiographs: primary, reactivation (also called secondary or post-primary infection), and miliary.

A first exposure to *M. tuberculosis* leads to primary TB, which has a nonspecific imaging appearance. It can be manifested by a homogenous consolidation, lymphadenopathy, or even a pleural effusion. Often, these findings will resolve, but in some cases a residual Ghon focus, or a calcified caseating granuloma, can be noted on radiography [43, 44]. Primary TB in children, for example, most often presents with lymph node enlargement, often unilateral hilar nodes, seen in 90–95% of cases [45, 46]. In contrast, the most common radiographic manifestation of reactivation pulmonary TB is focal or patchy heterogeneous consolidation involving the apical and posterior segments of the upper lobes and the superior segments of the lower lobes. Another common finding is the presence of poorly defined nodules and linear opacities, which are seen in approximately 25% of patients [45]. Cavities, the radiologic hallmark of reactivation TB, are

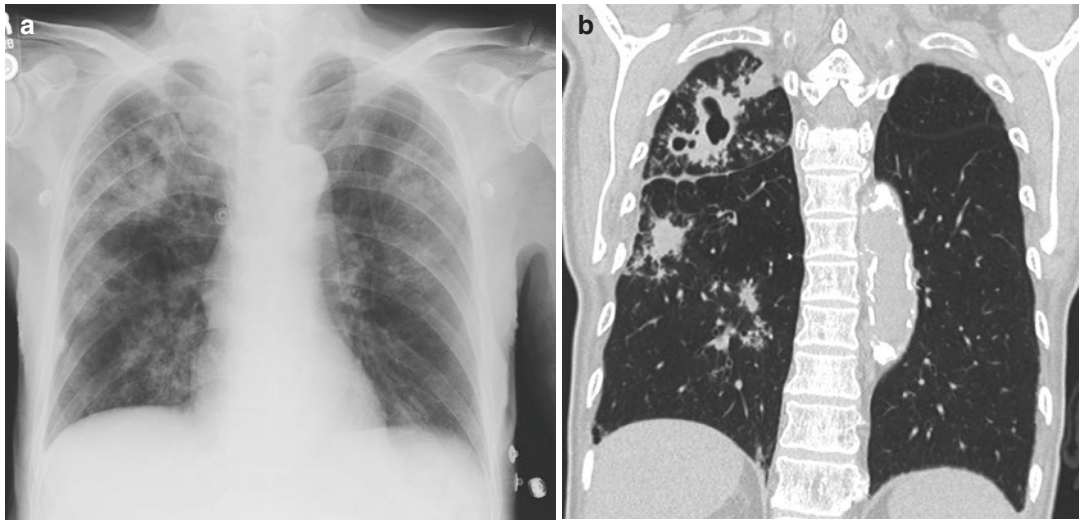

Fig. 16.5 Frontal radiograph (**a**) and coronal CT chest (**b**) in a 79-year-old male with right upper lobe thick-walled cavitary structures found to have reactivation TB

evident radiographically in 20–45% of patients (Fig. 16.5) [42]. Finally, in cases of miliary TB, the chest radiograph may demonstrate characteristic innumerable 1–3 mm diameter nodules randomly distributed throughout both lungs; thickening of interlobular septa is also frequently present [1, 45] (Fig. 16.6).

As TB can notably present with a normal chest radiograph, CT is an important modality for early diagnosis and in guiding management. Both in later stages of TB or during treatment, CT imaging can reveal early cavitation, pleural and pericardial effusions, lymphadenopathy, and other findings, which may not be suspected on chest radiographs [47].

TB is an infection that is not only confined to the lungs but has a tendency to proliferate throughout the body. In the heart, TB is known to cause pericardial effusions (Fig. 16.7) and pericarditis. Pericardial effusions can be diagnosed by echocardiography or by point-of-care ultrasound [48].

TB can also affect any organ or tissue in the abdomen and can be mistaken for other inflammatory or neoplastic conditions [49]. The most common sites of abdominal TB are lymph nodes; typical findings include lymphadenopathy with central low attenuation due to the presence of perinodal granulation tissue and central caseous necrosis [49]. Peri-portal and para-aortic lymphadenopathy are easily identified on ultrasound using the previously described FASH technique for the diagnosis of extrapulmonary TB in the setting of HIV (Fig. 16.8). Other sites that are affected include the genitourinary tract, peritoneal cavity, and gastrointestinal tract. In an HIV patient, the liver, spleen, biliary tract, pancreas, and adrenals are also commonly involved [49].

Central nervous system (CNS) TB is thought to occur in 2–5% of those infected with TB [43, 50] and can occur due to local or hematogenous spread. Infection can lead to varying manifestations, of which tuberculous meningitis and an intracranial tuberculous granuloma are the most common. Tuberculous meningitis most often presents with thick leptomeningeal enhancement at the base of the brain, which can result in obstructive hydrocephalus [43]. Tuberculous granulomas present as ring-enhancing lesions with surrounding edema, again more likely at the base of the brain, with or without associated meningeal enhancement [51]. These findings can be noted on contrast-enhanced CT or MRI (Fig. 16.9).

Tuberculous spondylitis, or Pott disease, is a common manifestation of TB in the spine, infecting the vertebral body and intervertebral disc.

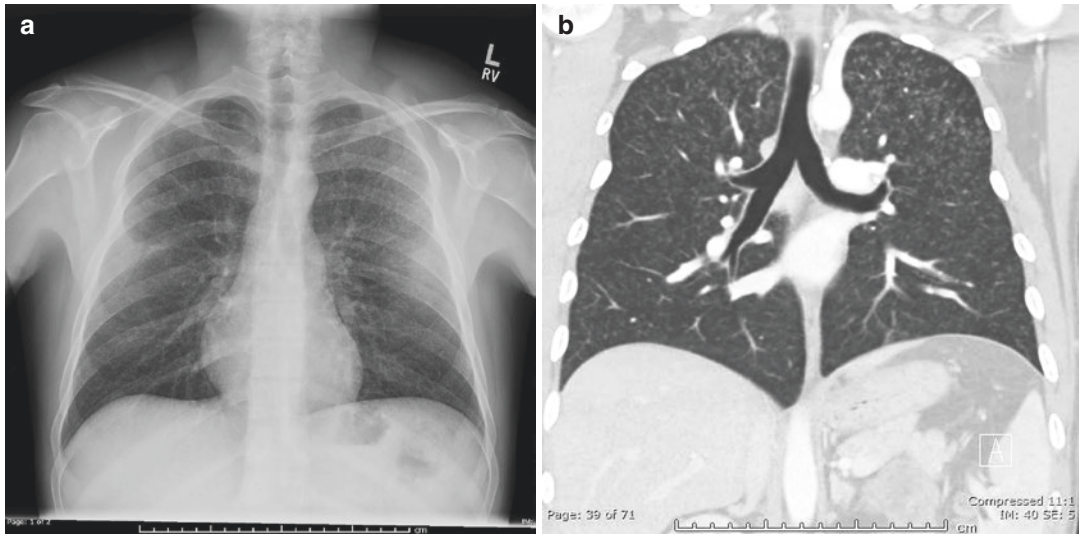

Fig. 16.6 Frontal radiograph (**a**) and coronal CT chest (**b**) demonstrating diffuse bilateral reticulonodular opacities in a 28-year-old male patient with miliary pattern of disseminated TB infection. (Images courtesy of Shaden Mohammad, MD)

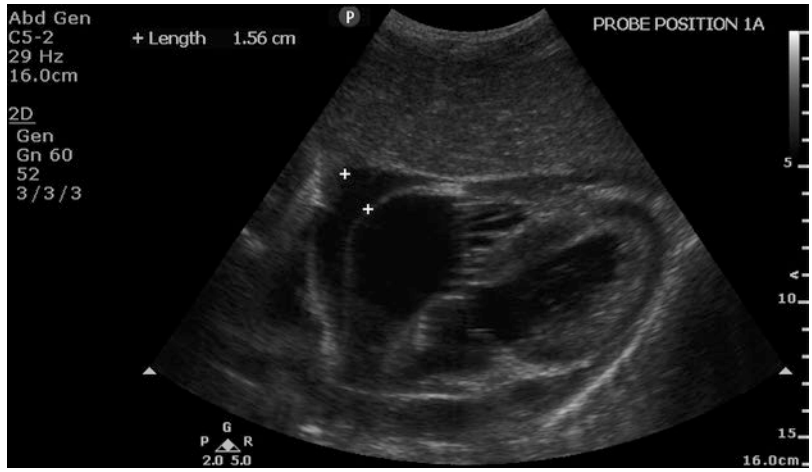

Fig. 16.7 FASH protocol subxiphoid image of the heart demonstrates pericardial effusion in a 36-year-old male due to TB

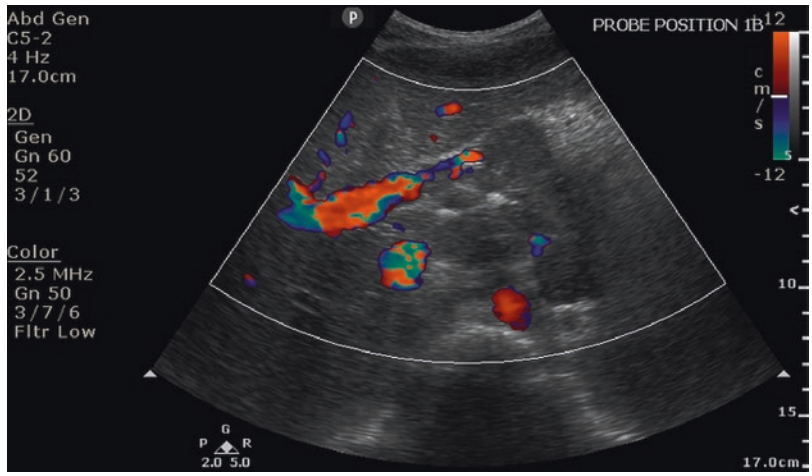

Fig. 16.8 FASH protocol transverse image of the upper mid-abdomen in a 28-year-old male demonstrates matted hypoechoic para-aortic and peri-portal lymphadenopathy due to extrapulmonary TB

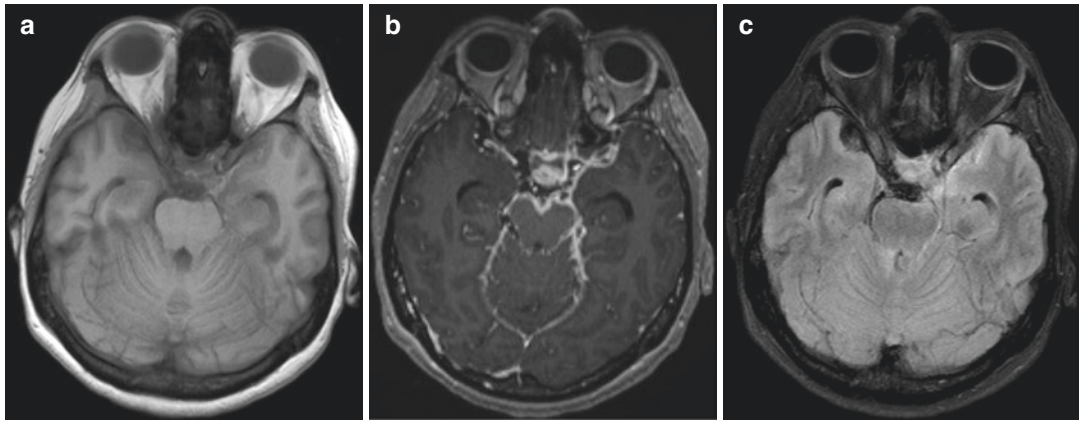

Fig. 16.9 Axial pre- (**a**) and post-contrast (**b**) T1-weighted and FLAIR (**c**) images through the base of the brain demonstrate thick, basilar meningeal enhancement in a 34-year-old female with AIDS, found to have TB meningitis

In the early stages and to assess the extent of involvement, MRI is the preferred modality. In later stages, reduction in vertebral body height, sclerotic vertebral bodies, or even compression deformities can be seen [43].

Tuberculosis: Differential Considerations

As in other endemic infections, the genitourinary (GU) tract is commonly involved in TB. Differentiation from other causes of calcification seen in the GU tract, such as in schistosomiasis, is often possible only in the later stages of the disease(s). For example, in schistosomiasis, calcification is first seen in the lower end of the ureters and the bladder and then extends *up* the ureters. In TB, the calcification extends *down* the ureters and the bladder, affecting the kidney much more often (Fig. 16.10) [52].

Another endemic parasitic infection commonly diagnosed on chest radiographs is paragonimiasis. The disease is most prevalent in populations of Asia (Korea, Japan, Taiwan, central and southern China, and the Philippines) as well as Mexico and South America (Brazil, Costa Rica, Honduras) [1]. Since 2001, the number of new cases of paragonimiasis has alarmingly increased in much of coastal Asia and Japan and has emerged as a significant public health issue [53]. Some of those with *Paragonimus* infections

Fig. 16.10 Coronal CT through the abdomen and pelvis of an 83-year-old male demonstrating multiple dense calcifications replacing much of the left kidney. This appearance is also referred to colloquially as "putty kidney"

are symptom-free and unaware of their infection; others develop a chronic cough and chest pain, classically describing "chocolate-colored" sputum [1]. Hemoptysis can often occur irregularly and continue for years. The life cycle of this species of trematode predicates maturation to adulthood in snails and other shellfish and subsequently infects humans via ingestion due to poor water sanitation or undercooked seafood. The eggs hatch in the gastrointestinal tract and larvae migrate throughout the body, mainly to the lungs and pleural cavity to continue the life cycle.

On CT, pulmonary paragonimiasis presents as a subpleural or subfissural nodule with a necrotic low-attenuation area. Additional findings include subpleural linear opacities, presumably worm migration tracks, leading to necrotic and peripheral pulmonary nodules, adjacent bronchiectasis, areas of ground-glass attenuation, pleural effusion, and pneumothorax [54]. Later findings are thought to be caused by worm cysts and include solitary or multiple nodules or gas-filled cysts [55].

The radiographic appearance can make differentiation of pleuropulmonary *Paragonimus* and TB difficult in areas of the world where both infections are endemic; differentiation may require sputum or lesion tissue pathologic examination [56] (Fig. 16.11).

Melioidosis, a deadly gram-negative bacterial infection found primarily in Southeast Asia, can also cause a TB-like pattern of disease [1]. Pulmonary involvement is reported to be the most common form of melioidosis, accounting for >50% of cases. Melioidosis is often first noted on chest radiographs [57, 58] and can be easily confused with TB. A high index of suspicion is therefore required to make this diagnosis. In acute, nonsepticemic, pneumonic melioidosis, the most common radiographic pattern is focal consolidation with or without cavitation. As might be seen in primary TB, melioidosis typically begins in the upper lobes, often quickly spreading to other lobes, and forms nodules or patchy densities. Compared to TB, rapid clinical and radiographic progression with early cavitation favors melioidosis; hilar adenopathy is rarely seen in melioidosis [1].

Schistosomiasis

One of the most common and insidious endemic infectious diseases throughout southeastern Asia, coast South America, and Africa is schistosomiasis. More than 90% of patients requiring treatment for schistosomiasis reside in Africa [59]. There are two major forms of infection with schistosomiasis, intestinal and genitourinary. As discussed previously, genitourinary schistosomiasis presents with bladder and distal ureteral calcifications that extend retrograde. In the intestine, schistosomiasis presents with intestinal wall calcifications, which can be seen on CT [60]. For the diagnosis of hepatosplenic schistosomiasis, however, ultrasound is the preferred modality. Findings include peri-portal fibrosis, reduced portal blood flow, varices, and splenomegaly [60, 61] (Fig. 16.12).

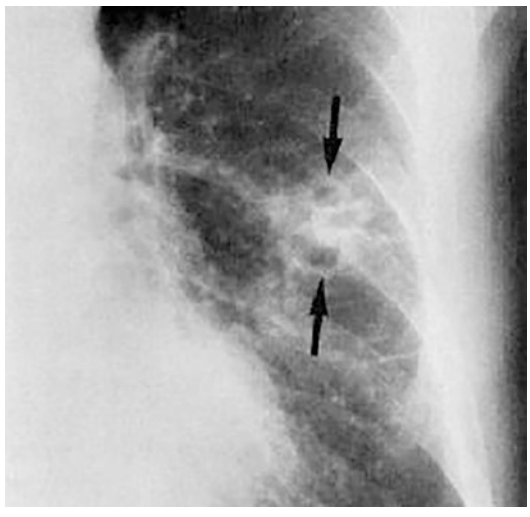

Fig. 16.11 Focal view of a left mid-lobe lesion demonstrating multiple small aggregated cysts in a patient with *Paragonimus* (arrows) [9]. (Reprinted from Lungren et al. [9], with permission from SpringerNature)

Fig. 16.12 Anteroposterior (AP) radiograph of the pelvis demonstrating thick circumferential calcification of the bladder and distal ureters, which are dilated in a patient with long-standing schistosomiasis infection. A large calcified bladder stone is also present [9]. (Reprinted from Lungren et al. [9], with permission from SpringerNature)

Echinococcus

Echinococcus granulosus is a cyst-forming tapeworm especially prevalent in parts of Asia, north and east Africa, Australia, and South America that is known to cause echinococcosis or hydatid disease, one of the most common hepatobiliary infections in the world. The tapeworm's life cycle involves dogs as definitive hosts and sheep, pigs, goats, horses as intermediate hosts; humans become inadvertent intermediate hosts after ingestion of the eggs excreted by infected dogs. The hatched larvae travel to the liver where they form fluid-filled hydatid cysts. Over time, daughter cysts may develop. In addition, an inflammatory granulomatous and/or fibrotic reaction may also occur [62]. The infection is endemic worldwide, with the highest prevalence in sheep-raising communities. Because of the wide prevalence, hydatid liver disease must be considered in the differential diagnosis of a cyst or mass in virtually any patient who is residing in, or has traveled through, an endemic area [1]. Ultrasound is highly helpful in the diagnosis/classification of hydatid liver disease, and a grading scale has been developed by the WHO [63] (Fig. 16.13). While MRI is increasingly being used in the advanced health systems, ultrasound of the liver remains the most cost-effective and available in the developing world. Unfortunately, ultrasonography is not always able to differentiate hydatid cysts from tumors or liver abscesses, and additional imaging, such as CT or MRI, may still be required (Fig. 16.14).

The tapeworm also affects the lungs and is, in fact, reported to be the most common parasitic lung infection worldwide [1]. It can present as a cavitary lung lesion, often containing smaller collections referred to as "daughter cysts" [32, 64]. They are often asymptomatic and recognized incidentally on CT [1, 65].

Chagas Disease (South America)

The parasite *Trypanosoma cruzi* causes Chagas disease (American trypanosomiasis) and is estimated to have infected 8 million people, predominantly in Latin America [66]. Chagas

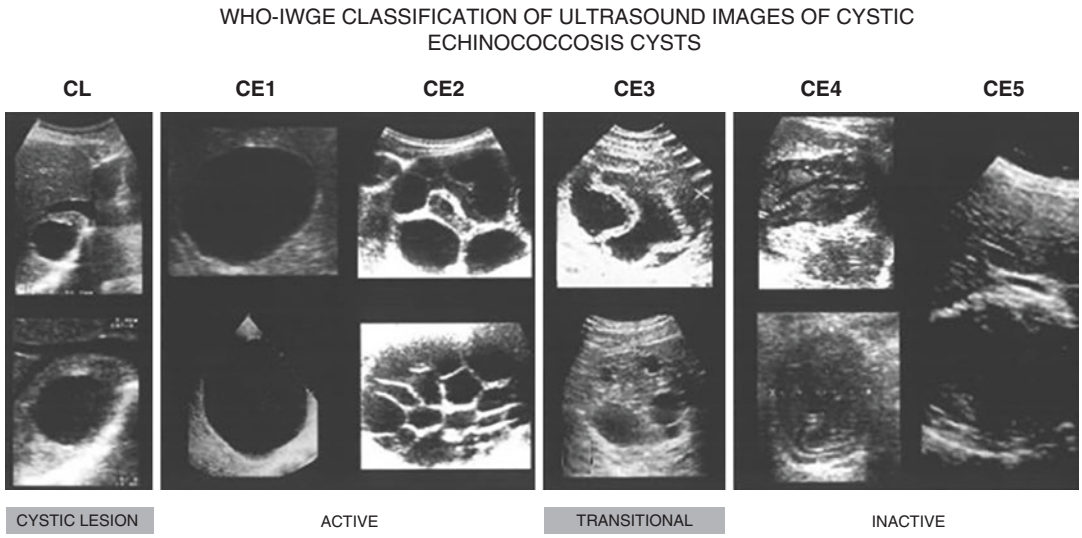

Fig. 16.13 WHO cystic echinococcosis (CE) grading scale by ultrasound. The classification is intended to follow the natural history of CE and starts with undifferentiated simple cysts, as presumably hydatid cysts evolve from these structures. The first clinical group starts with cyst types CE 1 and 2 and such cysts are active, usually fertile containing viable organisms. CE type 3 are cysts entering a transitional stage where the integrity of the cyst has been compromised either by the host or by chemotherapy and this transitional stage is assigned to the second clinical group. The third clinical group comprises CE types 4 and 5 which are inactive cysts which have lost their fertility and are degenerative [9]. (Reprinted from Lungren et al. [9], with permission from SpringerNature)

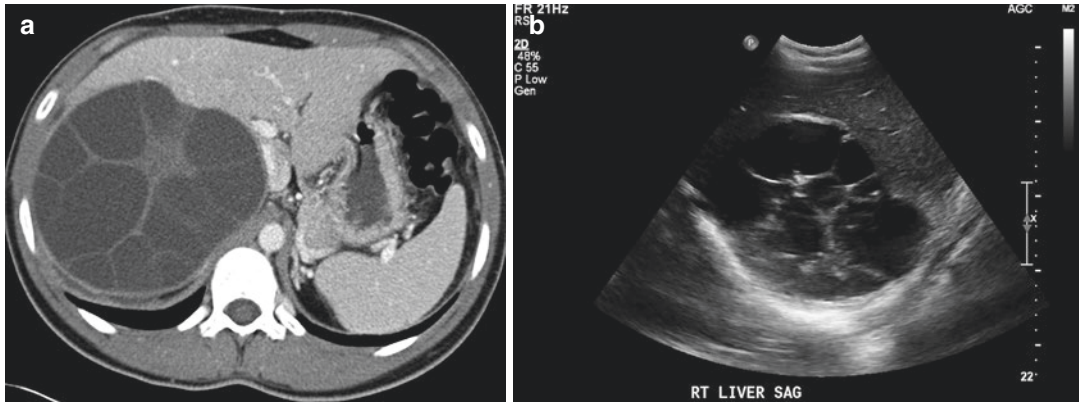

Fig. 16.14 Axial CT image (**a**) and sagittal ultrasound (**b**) of the liver of a 19-year-old male with hydatid liver disease. The CT demonstrates a large multiseptated, cystic lesion in the liver, and the ultrasound shows the same cyst's multiseptated, hypoechoic appearance

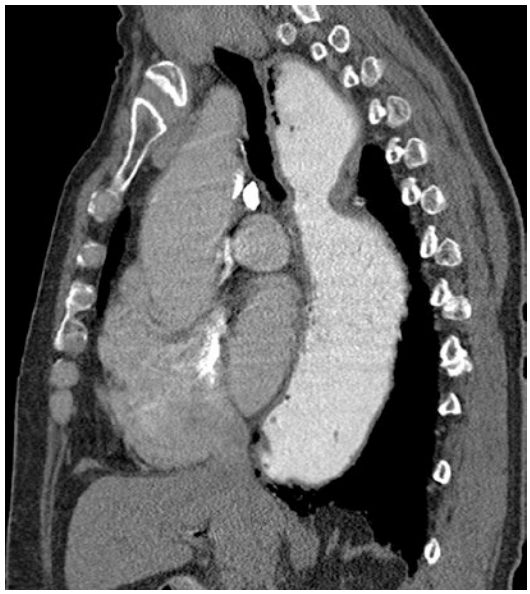

Fig. 16.15 Sagittal CT with oral contrast of a 78-year-old female patient with Chagas disease of the esophagus. The image demonstrates as significantly dilated, contrast-filled esophagus

disease can present with severe esophageal dysfunction; trypomastigotes, the differentiated offspring of the parasite, tend to invade the esophagus and give rise to a megaesophagus and/or achalasia (Fig. 16.15), which can be visualized with a lateral radiograph during a barium contrast esophagram. Chagas disease can also cause dilation of other segments of the gastrointestinal tract, particularly the proximal small bowel and the colon in severe cases, and can also be diagnosed with fluoroscopic and/or barium contrast studies [1].

Chagas disease may cause myocarditis in up to 5% of infected patients in the acute phase which can be cured with oral anti-trypanosomal medication [67, 68]. The acute-phase myocarditis can be diagnosed by echocardiography. Although unable to delineate the etiology, echocardiography is able to demonstrate cardiac function and can be used to track the progression of disease [67]. Many acute-phase Chagas infections are underdiagnosed or unrecognized. Approximately 30% of untreated patients progress to chronic-phase Chagas disease which can manifest as chronic Chagas cardiomyopathy (CCC). CCC can lead to progressive heart failure and sudden cardiac death. Cardiac MRI is not widely available in resource-poor regions but may detect myocardial involvement in untreated chronic Chagas disease [69–71].

Roundworms

Roundworms fall under a sub-group of soil-transmitted helminth infections and are exceedingly common in many parts of the world. More

than 20% of the world's population is thought to have been infected with this type of parasite [72]. Infection due to *Ascaris lumbricoides* (termed ascariasis) is acquired by ingesting contaminated water or food that contains embryonated eggs. Numerous investigators have observed that the highest rate of infection with *Ascaris* is in children between 1 and 15 years of age. In hot and humid areas of rural Africa, Asia, and Latin America, up to 93% of all inhabitants in some villages may be infected [1, 37, 52]. While the diagnosis is mainly dependent on examination of stool samples, barium contrast agents are helpful in evaluating the presence of roundworm infection in the gastrointestinal tract (Fig. 16.16). In heavily infested patients, large collections of ascarids can frequently be identified on abdominal radiography without oral contrast [1, 73, 74]. In fact, large masses of worms in the bowel are best seen as a tangled group of thick cords and sometimes produce a "whirlpool" effect (Fig. 16.17). It is important to keep in mind the epidemiology of the region, as the differential diagnosis for an intraluminal worm identified by imaging is relatively nonspecific and can also represent a variety of other parasitic worm infections or noninfectious etiologies. Note that other worm infections, such as hookworms (*A. duodenale* and/or *N. americanus*), whipworms (*T. trichiura*), and capillariasis (*C. philippinensis*), are typically characterized on enterography by the inflammation or other changes in the bowel rather than direct visualization of the worms themselves due to their small size (10 mm on average in the case of *A. duodenale*). Stool examination and evaluation for worms and/or ova is diagnostic.

Leprosy

One of the most notorious and stigmatized infections in LMICs is leprosy, a chronic and debilitating infection caused by *Mycobacterium leprae*, which often in late stages dramatically manifests as skeletal changes. There are an estimated one million patients with leprosy in the world, and

Fig. 16.16 Barium examination of the stomach clearly demonstrates the outlines of individual ascarids (worms) as elongated radiolucent-filling defects within the barium column [9]. (Reprinted from Lungren et al. [9], with permission from SpringerNature)

Fig. 16.17 AP abdominal radiograph demonstrates a large bolus of worms in the cecum causing intestinal obstruction, manifest as thick tangles of cords within the air-filled large bowel [9]. (Reprinted from Lungren et al. [9], with permission from SpringerNature)

while radiology is not often necessary for an initial diagnosis, imaging does play a vital role in assessing the activity and extent of the disease and in helping to plan surgery and rehabilitation [1, 75]. The highest prevalence is in India and tropical Africa and South America; it also still occurs frequently in Southeast Asia, the Philippines, southern China and southern Malaysia, Indonesia, and some of the South Pacific islands [1, 75]. Leprosy presents in many different ways, both clinically and pathologically, but generally is divided into two different types: tuberculoid leprosy and lepromatous leprosy. The two differ primarily in the immune response generated by the infection. The differences in this characteristic result in lepromatous leprosy being the more severe form, with full body manifestations [76]. Primary skeletal changes are most frequent in lepromatous leprosy, and the bone findings are essentially destructive patterns with very little surrounding bone reaction or sclerosis until healing occurs [1, 75] (Fig. 16.18). The disease is usually diagnosed clinically (symptoms, physical exam, and history), and radiographs are most commonly utilized to monitor complications of the infection, including secondary pyogenic osteomyelitis due to the ulceration and neuromuscular changes of the infection in the extremities.

Cysticercosis

Cysticercosis is prevalent in Africa, Asia, and Latin America. It is estimated to be the cause of 30% of epilepsy cases in regions where it is endemic [77]. Cysticercosis is acquired by ingesting food, water, or feces containing eggs of *T. solium*. The oncospheres (larvae) are released from their shells in the gut and invade throughout the body, developing into cysticerci, most commonly in the skeletal muscles and brain [1, 78].

Musculoskeletal involvement of *Taenia solium* (cysticercosis) infection can be readily diagnosed with radiography because the appearance is pathognomonic. They appear as oblong calcified foci parallel to the muscle fibers and have been described as rice grain calcifications. Calcified lesions have been demonstrated in up to 97% of patients examined 5 or more years after infection and can be easily demonstrated by radiographs of the extremities [1] (Fig. 16.19).

Patients with a central nervous system (CNS) infection with cysticercosis, or neurocysticercosis, present with seizures. Similar to the calcifications seen in skeletal muscle, head CT findings include multiple calcified lesions throughout the brain parenchyma measuring between 2 and 10 mm, with or without mass

Fig. 16.18 Lateral radiograph of the foot demonstrates the final stages of leprosy characterized by the large areas of bone absorption. As the talus disintegrates, with weight-bearing, there is complete disruption of the foot, leaving the patient vulnerable to secondary infections which, in combination, leave little normal anatomy or function [9]. (Reprinted from Lungren et al. [9], with permission from SpringerNature)

Fig. 16.19 Frontal plain film radiograph of the bilateral knees of a 57-year-old female demonstrates calcifications in the soft tissues and muscles. The calcified cysticerci are aligned with their long axes in the plane of the muscle bundles of the legs

Fig. 16.20 Axial non-contrast head CT demonstrates multiple parenchymal calcified lesions, some with mild surrounding edema characteristic of the nodular calcified stage of cysticercosis [9]. (Reprinted from Lungren et al. [9], with permission from SpringerNature)

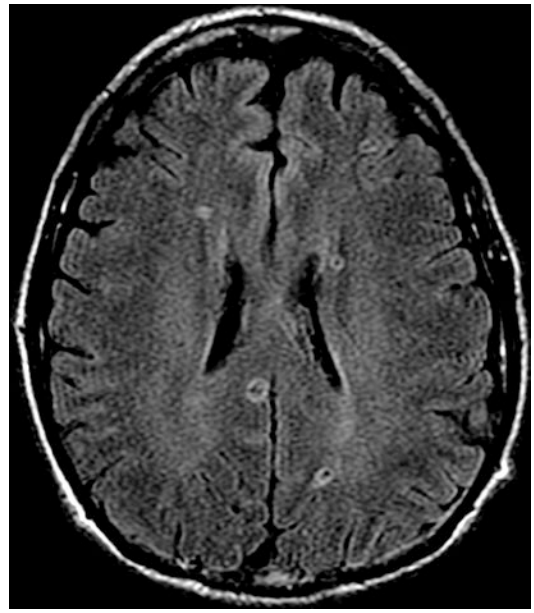

Fig. 16.21 Axial FLAIR brain MR of a 61-year-old Ecuadorian male demonstrates thin-walled cysts, one of which has a mural nodule. This is the vesicular stage of neurocysticercosis. (Image courtesy of Kevin Spitler, MD)

effect or contrast enhancement (Fig. 16.20). Treatment of cysticercosis depends on the form and the type of disease and the location and number of cysts [1, 79].

There are four main stages of neurocysticercosis. In the vesicular stage, the parasite is still viable and has an intact membrane, resulting in no reaction within the host. The cyst can be visualized on CT and MRI without significant associated enhancement on post-contrast images. The next stage is called the colloidal vesicular stage, in which the parasite dies with or without treatment. At this point, the cyst membrane is no longer intact, causing surrounding edema and cyst wall enhancement. In the granular nodular stage, this edema diminishes and the cyst retracts with persistent enhancement. In the nodular calcified stage, a calcified cyst can be seen on non-contrast CT without surrounding edema [80].

Although unlikely to be the most financially feasible or an available option in many regions, MRI is able to reveal even small cysts (Fig. 16.21). In addition, the accompanying edema is often well demonstrated on T2-weighted or fluid-attenuated inversion recovery (FLAIR) MRI sequences. MRI is also the study of choice for evaluation of ventricular neurocysticercosis, which is often impossible to diagnose by CT. The intraventricular cystic lesions are generally isointense to cerebrospinal fluid (CSF) and may demonstrate a thin hypointense rim particularly with T2-weighted sequences. Clinically, this form of neurocysticercosis is important to recognize as these lesions can grow to occlude the CSF, potentially leading to acute hydrocephalus and sudden death (Fig. 16.22).

Toxoplasmosis

One of the most widespread parasitic infections in the world is toxoplasmosis, caused by *Toxoplasma gondii*, a protozoan that infects humans and commonly involves the CNS. It is estimated that approximately 95% of the world

has been infected with *Toxoplasma* [81]. It has a complex life cycle, but infection is most commonly via inadvertent ingestion of oocysts, often shed by domesticated cats, but also can be ingested via eating raw or undercooked meat, plants contaminated with oocysts, and unpasteurized dairy products and can be caused by organ transplantation and congenital transplacental infection. The oocysts hatch and the sporozoites quickly become widely distributed within the host blood stream and intestines. The preferred extra-intestinal sites for *T. gondii* include skeletal and heart muscle, brain, and other tissues of the CNS.

Fig. 16.22 Saggital T1-weighted MR image demonstrates a large cyst due to cysticercosis in the trigone of the right lateral ventricle [9]. (Reprinted from Lungren et al. [9], with permission from SpringerNature)

A CNS *Toxoplasma* infection is termed "neurotoxoplasmosis" and most often occurs in immunocompromised patients, including those with HIV/AIDS. On CT, this manifests as multiple, variable-sized, ring-enhancing hypodense regions, predominantly in the basal ganglia and at the corticomedullary junction (Fig. 16.23). These lesions will also demonstrate ring enhancement on post-contrast MRI [82].

Toxoplasmosis can undergo transplacental transmission from an infected mother to fetus. In most cases, this infection is asymptomatic. In those cases with symptomatic presentation, manifestations depend upon the timing of infection during pregnancy. On fetal ultrasound, the most common findings include fetal hydrocephalus and intracranial parenchymal calcifications.

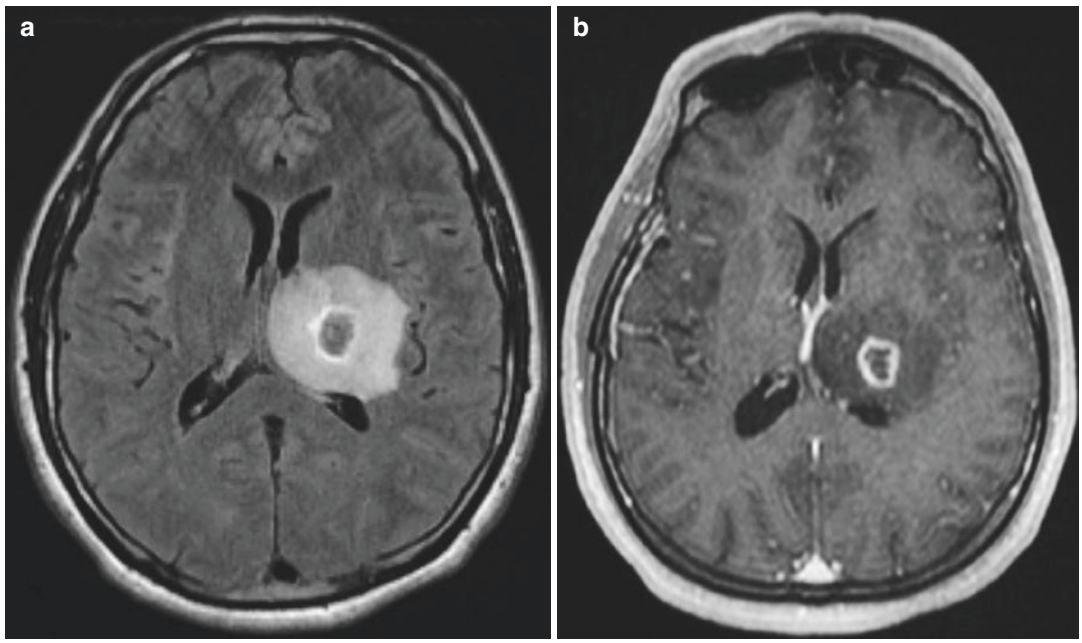

Fig. 16.23 Axial FLAIR brain MR (**a**) and axial post-contrast T1-weighted brain MR (**b**) in a 34-year-old male with AIDS demonstrates ring-enhancing lesions with surrounding edema consistent with toxoplasmosis brain abscess

Additional findings include intrahepatic calcifications, ascites, and hepatosplenomegaly [83].

Clonorchiasis

Clonorchiasis, also known as Chinese liver fluke disease, is caused by *Clonorchis sinensis* and is endemic to eastern China and southeastern Asia. Adult flukes infect dogs and other fish-eating carnivores, eventually infecting humans where they migrate into bile ducts and complete the life cycle [84]. Infection leads to recurrent pyogenic cholangitis, biliary strictures, and cholangiocarcinoma. Both ultrasound and CT demonstrate uniform intrahepatic dilatation of small bile ducts with relative sparing of large bile ducts. The flukes cannot be visualized on imaging. Chronic clonorchiasis results from protracted episodes of re-infection over time. Treatment of this chronic infection is important because of its strong association with cholangiocarcinoma [85, 86].

Entamoeba histolytica

Infection with *Entamoeba* is relatively widespread throughout much of the developing world. It is thought that approximately 8% of those in endemic regions are exposed and approximately 90% of those become symptomatic, resulting in an estimated 100,000 deaths annually [87]. *Entamoeba* is an amoebic parasite that is ingested orally and can invade the large bowel and progress from there to cause extra-intestinal infection. On ultrasound, extra-intestinal amebiasis most commonly presents as a single, hypoechoic liver lesion with a rim or capsule; this is known as an amebic liver abscess. This needs to be differentiated from a pyogenic liver abscess caused by biliary tree infections, diverticulitis, or abdominal interventions. These may mimic amebic liver abscesses on ultrasound, but pyogenic abscesses tend to be more variable in shape, are often multiple, and may have regions of markedly increased echogenicity representing gas bubbles (Fig. 16.24), all of which are not usually noted with amebiasis [23].

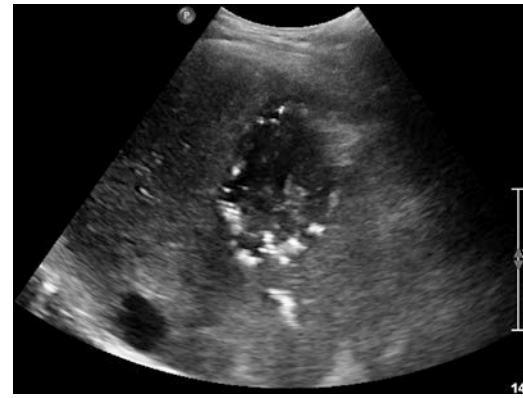

Fig. 16.24 Transverse view of the right upper quadrant in a 47-year-old male with colon cancer demonstrates a hypo- to anechoic lesion with irregular borders and echogenic foci representing gas bubbles consistent with a pyogenic abscess

Zika

Over recent years, Zika virus has come to the forefront of popular attention. Zika is a virus spread primarily by mosquitos of the *Aedes* species, generally causing only minor symptoms in those infected directly. Unfortunately, however, during pregnancy, the virus can be transmitted vertically to fetuses from infected mothers, causing primarily CNS abnormalities. Retrospective analyses of fetal ultrasound and MRI demonstrated normal fetal cerebral parenchymal development up to 24 weeks. Thereafter, decreased growth rate of fetal head circumference, asymmetry between abdominal and head circumference, increased nuchal skin fold thickness, neural cortical abnormalities, corpus collosum abnormalities, cerebral hemisphere hypoplasia, brainstem hypoplasia, calcifications in the gray-white matter junction, and posterior fossa abnormalities were observed on imaging [88–90]. Many of these findings can be seen on fetal ultrasound or MRI. At the time of birth, some of these findings can be seen on neonatal cranial ultrasound which can be obtained in resource-poor regions. Further evaluation of high-risk newborns, however, should include a head CT or brain MRI at a tertiary center with expertise in neuroradiology.

Other congenital infections include the TORCH infections. TORCH is an acronym

standing for toxoplasmosis, other (syphilis, varicella-zoster, parvovirus B19), rubella, cytomegalovirus, and herpes infections. TORCH infections account for 2–3% of all congenital abnormalities [91]. Many of the neuro-imaging findings described above for Zika can also be seen in the TORCH infections. For this reason, it is important to obtain polymerase chain reaction (PCR) confirmation of Zika virus infection prenatally or in the neonate with presumed infection (Figs. 16.25, 16.26, and 16.27).

Conclusion

Globally, infectious diseases make up a significant portion of treatable causes of morbidity and mortality. Imaging is essential in the diagnosis and management of many of these diseases. It also places a significant role in the monitoring and reporting of outbreaks and identifying public health threats.

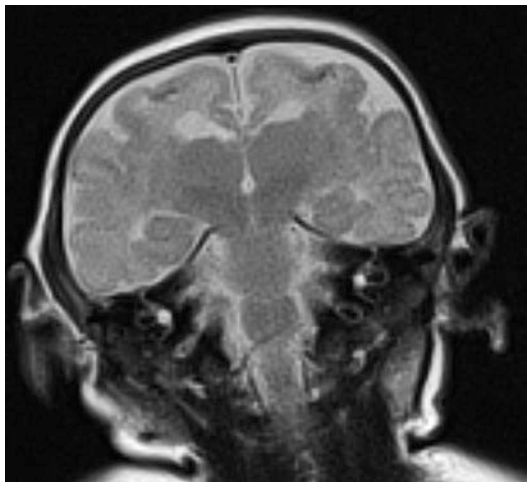

Fig. 16.25 Coronal T2-weighted images through the brain demonstrating T2 dark punctate calcifications at the gray-white junction and lissencephaly in a neonate with Zika virus infection. (Image courtesy of Karin Nielsen, MD, MPH)

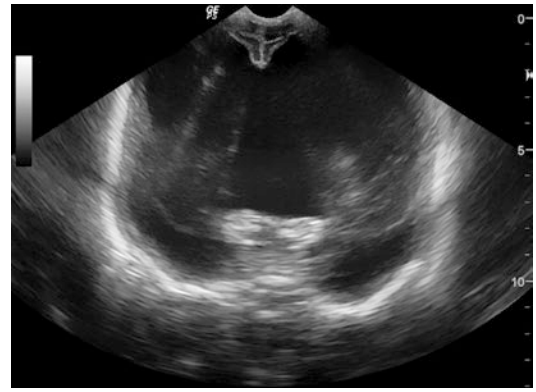

Fig. 16.27 Coronal head ultrasound demonstrating severe parenchymal volume loss and severe hydrocephalus in a neonate with Zika virus infection. (Image courtesy of Karin Nielsen, MD, MPH)

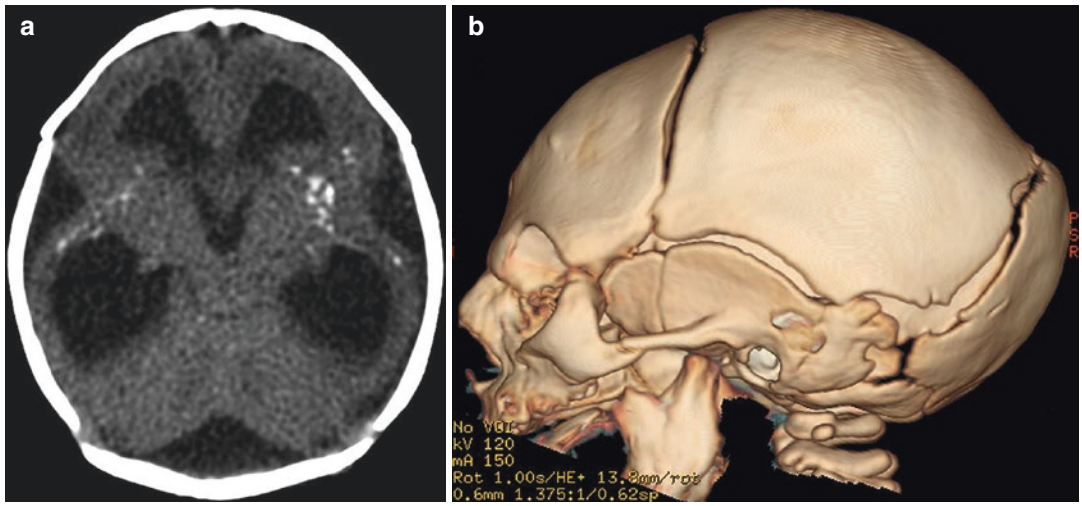

Fig. 16.26 Axial non-contrast CT (**a**) through the brain with 3D reconstruction (**b**) demonstrating microcephaly, hydrocephalus, lissencephaly, cerebellar abnormalities, basal ganglia calcifications, and calcifications at the gray-white junction in a neonate with Zika virus infection. (Images courtesy of Karin Nielsen, MD, MPH)

References

1. Palmer PES, Reeder MM. The imaging of tropical diseases: with epidemiological, pathological, and clinical correlation. 2 revised ed. Berlin: Springer; 2001.
2. WHO: Number of deaths: WORLD by cause; 2015. http://www.who.int/mediacentre/factsheets/fs310/en/.
3. MRG. European diagnostic imaging system market will grow modestly to almost $2.2 billion in 2017; 2013. https://www.prnewswire.com/newsreleases/european-diagnostic-imaging-system-market-will-grow-modestly-to-almost-22-billion-in-2017-191188891.html.
4. WHO: Global Maps for Diagnostic Imaging; 2014. http://www.who.int/diagnostic_imaging/collaboration/global_collab_maps/en/.
5. Frost & Sullivan. Brazilian medical imaging market growth driven by socio-economic factors and private investments; 2013. https://www.prnewswire.com/news-releases/european-diagnostic-imaging-system-market-will-grow-modestlyto-almost-22-billion-in-2017-191188891.html.
6. Frost & Sullivan. CEE and Russia medical imaging market forecasted to rise at $2.34 billion in 2015; 2013. https://www.prnewswire.com/news-releases/european-diagnostic-imaging-system-market-will-grow-modestlyto-almost-22-billion-in-2017-191188891.html.
7. Ken Research Private Ltd. India Medical Imaging Industry Outlook to 2017—led by surging income and low penetration; 2013. http://www.kenresearch.com/healthcare/medicaldevices-and-equipments/india-medical-imaging-industry-research-report/374-91.html.
8. Ken Research Private Ltd. Asia Pacific medical imaging industry outlook to 2017—driven by rising lifestyle diseases and public healthcare expenditure; 2013. http://www.researchandmarkets.com/reports/2556859/asia_pacific_medical_imaging_industry_outlook_to.
9. Lungren MP, Peper JPC, Ordoñez AA, Jain SK. Infectious disease imaging. In: Mollura DP, Lungren MP, editors. Radiology in global health. 1st ed. New York: Springer; 2014. p. 159–80.
10. Mansfield P, Maudsley AA. Medical imaging by NMR. Br J Radiol. 1977;50:188–94.
11. Santiago Restrepo C, Gimenez CR, McCarthy K. Imaging of osteomyelitis and musculoskeletal soft tissue infections: current concepts. Rheum Dis Clin N Am. 2003;29:89–109.
12. Dai J. Opportunities and challenges of MRI in the developing world. Proc Int Soc Mag Reson Med. 2006:14.
13. Török E, Moran E, Cooke F. Cerebral abscess. In: Oxford handbook of infectious diseases and microbiology. Oxford: Oxford University Press; 2010. p. 771.
14. Bourne R. Fundamentals of digital imaging in medicine. London: Springer; 2010.
15. Török E, Moran E, Cooke F. Cestodes. In: Oxford handbook of infectious diseases and microbiology. Oxford: Oxford University Press; 2010. p. 604–6.
16. Koh DM, Burke S, Davies N, SPG P. Transthoracic US of the chest: clinical uses and applications. Radiographics. 2002 Jan-Feb;22(1):e1.
17. Bureau NJ, Chhem RK, Cardinal E. Musculoskeletal infections: US manifestations. Radiographics. 1999;19(6):1585–92.
18. Shah S, Noble VE, Umulisa I, et al. Development of an ultrasound training curriculum in a limited resource international setting: successes and challenges of ultrasound training in rural Rwanda. Int J Emerg Med. 2008;1:193–6.
19. Maru DS, Schwarz R, Jason A, Basu S, et al. Turning a blind eye: the mobilization of radiology services in resource-poor regions. Glob Health. 2010 Oct 14;6:18.
20. Groen RS, Leow JJ, Sadasivam V, Kushner AL. Review: indications for ultrasound use in low- and middle-income countries. Tropical Med Int Health. 2011;16:1525–35.
21. Shah SP, Epino H, Bukhman G, et al. Impact of the introduction of ultrasound services in a limited resource setting: rural Rwanda 2008. BMC Int Health Hum Rights. 2009;9:4.
22. Spencer JK, Adler RS. Utility of portable ultrasound in a community in Ghana. J Ultrasound Med. 2008;27:1735–43.
23. Belard S, Tamarozzi F, Bustinduy AL, et al. Review article: point-of-care ultrasound assessment of tropical infectious diseases – a review of applications and perspectives. Am J Trop Med Hyg. 2016;94(1):8–21.
24. Condeelis J, Weissleder R. In vivo imaging in cancer. Cold Spring Harb Perspect Biol. 2010;2:a003848.
25. Hammoud DA, Hoffman JM, Pomper MG. Molecular neuroimaging: from conventional to emerging techniques. Radiology. 2007;245:21–42.
26. Signore A. The developing role of cytokines for imaging inflammation and infection. Cytokine. 2000;12:1445–54.
27. Baum R. Theranostics, Gallium-68, and other radionuclides: a pathway to personalized diagnosis and treatment. Berlin: Springer; 2013.
28. Esmail H, Lai RP, Lesosky M, et al. Characterization of progressive HIV-associated tuberculosis using 2-deoxy-2-[18F]fluoro-D-glucose positron emission and computed tomography. Nat Med. 2016;22(10):1090–3.
29. Berezin EN, de Moraes JC, Hong T, et al. Pneumonia hospitalization in Brazil from 2003 to 2007. Int J Infect Dis. 2012;16:e583–90.
30. Török E, Moran E, Cooke F. Retropharyngeal abscess. In: Oxford handbook of infectious diseases and microbiology. Oxford: Oxford University Press; 2010. p. 634.
31. Török E, Moran E, Cooke F. Infective endocarditis. In: Oxford handbook of infectious diseases and microbiology. Oxford: Oxford University Press; 2010. p. 670.
32. Llewelyn H, Ang HA, Lewis KE, et al. Round opacity (or opacities) >5 mm in diameter. In: Oxford handbook of clinical diagnosis. Oxford: Oxford University Press; 2009. p. 728.

33. Török E, Moran E, Cooke F. Gas gangrene. In: Oxford handbook of infectious diseases and microbiology. Oxford: Oxford University Press; 2010. p. 792.
34. Tsai YF, Ku YH. Necrotizing pneumonia: a rare complication of pneumonia requiring special consideration. Curr Opin Pulm Med. 2012;18(3):246–52.
35. Allen CM, Al-Jahadi HH, Irion KL, et al. Imaging lung manifestations of HIV/AIDS. Ann Thoracic Med. 2010;5(4):201–16.
36. Tasaka S. Recent advances in the diagnosis of pneumocystis jirovecii pneumonia in HIV-infected adults. Expert Opin Med Diagn. 2013;7:85–97.
37. World Health Organization. Global tuberculosis report; 2016. http://www.who.int/tb/publications/global_report/gtbr13_executive_summary.pdf?ua=1.
38. CDC: Core Curriculum on Tuberculosis: What the clinician should know; 2016. https://www.cdc.gov/tb/education/corecurr/pdf/corecurr_all.pdf.
39. WHO: Frequently Asked Questions on Xpert MTB/RIF assay; 2014. http://www.who.int/tb/laboratory/xpert_faqs.pdf.
40. WHO: Chest Radiography in Tuberculosis Detection. 2016. http://apps.who.int/iris/bitstream/10665/252424/1/9789241511506-eng.pdf?ua=1.
41. Heller T, Wallrauch C, Goblirsch S, Brunetti E. Focused assessment with sonography for HIV-associated tuberculosis: a short protocol and pictorial review. Crit Ultrasound J. 2012;4(1):21.
42. Longmore M, Wilkinson IB, Davidson EH, et al. Clinical features of TB. In: Oxford handbook of clinical medicine. Oxford: Oxford University Press; 2010. p. 399.
43. Burrill J, Williams CJ, Bain G, et al. Tuberculosis: a radiologic review. Radiographics. 2007;27(5):1255–73.
44. Llewelyn H, Ang HA, Lewis KE, et al. Abnormal hilar shadowing—streaky. In: Oxford handbook of clinical diagnosis. Oxford: Oxford University Press; 2009. p. 742.
45. Jeong YJ, Lee KS. Pulmonary tuberculosis: up-to-date imaging and management. Am J Roentgenol. 2008;191:834–44.
46. Pool KL, Heuvelings CC, Belard S, Grobusch MP, Zar HJ, Bulas D, Garra B, Andronikou S. Technical aspects of mediastinal ultrasound for pediatric pulmonary tuberculosis. Pediatr Radiol. 2017 Dec;47(13):1839–48.
47. Török E, Moran E, Cooke F. Mycobacterium tuberculosis. In: Oxford handbook of infectious diseases and microbiology. Oxford: Oxford University Press; 2010. p. 407.
48. Patel MN, Beningfield S, Burch V. Abdominal and pericardial ultrasound in suspected extrapulmonary or disseminated tuberculosis. S Afr Med J. 2011 Jan;101(1):39–42.
49. Lee WK, Van Tonder F, Tartaglia CJ, et al. CT appearances of abdominal tuberculosis. Clin Radiol. 2012;67:596–604.
50. Kornienko VN, Pronin IN. Diagnostic neuroradiology. Berlin: Springer Verlag; 2009. p. 1288. ISBN:3540756523.
51. Kim TK, Chang KH, Kim CJ, et al. Intracranial tuberculoma: comparison of MR with pathologic findings. Am J Neuroradiol. 1995;16(9):1903–8.
52. Carrillo-Esper R, Moreno-Castaneda L, Hernandez-Cruz AE, et al. Renal tuberculosis. Cir Cir. 2010;78:442–7.
53. Mukae H, Taniguchi H, Matsumoto N, et al. Clinicoradiologic features of pleuropulmonary Paragonimus westermani on Kyusyu Island. Japan Chest. 2001;120:514–20.
54. Kim TS, Han J, Shim SS, et al. Pleuropulmonary paragonimiasis: CT findings in 31 patients. Am J Radiol. 2005;185:616–21.
55. Antimicrobe: Paragonimus species (Paragonimiasis); 2002. http://www.antimicrobe.org/b127rev2.asp.
56. Im JG, Whang HY, Kim WS, et al. Pleuropulmonary paragonimiasis: radiologic findings in 71 patients. Am J Roentgenol. 1992;159:39–43.
57. Burivong W, Wu X, Saenkote W, et al. Thoracic radiologic manifestations of melioidosis. Curr Probl Diagn Radiol. 2012;41:199–209.
58. Dhiensiri T, Puapairoj S, Susaengrat W. Pulmonary melioidosis: clinical-radiologic correlation in 183 cases in northeastern Thailand. Radiology. 1988;166:711–5.
59. WHO: Global Health Observatory (GHO) data: Schistosomiasis 2015. http://www.who.int/gho/neglected_diseases/schistosomiasis/en/.
60. Sah VK, Wang L, Min X, et al. Human schistosomiasis: a diagnostic imaging focused review of a neglected disease. Radiol Infect Dis. 2015;2:150–7.
61. Olveda DU, Olveda RM, Lam AK, et al. Utility of diagnostic imaging in the diagnosis and management of schistosomiasis. Clin Microbiol. 2014;3(2):142. pii: 142.
62. Nunnari G, Pinzone MR, Gruttadauria S, et al. Hepatic echinococcosis: clinical and therapeutic aspects. World J Gastroenterol. 2012;18:1448–58.
63. WHO Informal Working Group. International classification of ultrasound images in cystic echinococcosis for application in clinical and field epidemiological settings. Acta Trop. 2003;85:253–61.
64. Török E, Moran E, Cooke F. Cholecystitis and cholangitis. In: Oxford handbook of infectious diseases and microbiology. Oxford: Oxford University Press; 2010. p. 696.
65. Kilani T, El Hammami S. Pulmonary hydatid and other lung parasitic infections. Curr Opin Pulm Med. 2002;8:218–23.
66. WHO: Chagas disease (American trypanosomiasis). http://www.who.int/mediacentre/factsheets/fs340/en/.
67. Török E, Moran E, Cooke F. Ascariasis. In: Oxford handbook of infectious diseases and microbiology. Oxford: Oxford University Press; 2010. p. 591.
68. Acquatella H. Echocardiography in Chagas heart disease. Circulation. 2007;115:1124–31.
69. Lee-Felker SA, Thomas M, Felker ER, et al. Value of cardiac MRI for evaluation of chronic Chagas disease cardiomyopathy. Clin Radiol. 2016;71(6):618.e1–7.
70. Rochitte CE, Oliveira PF, Andrade JM, et al. Myocardial delayed enhancement by magnetic resonance imaging in patients with Chagas' disease: a marker of disease severity. J Am Coll Cardiol. 2005;46(8):1553e8. 9.
71. Gascon J, Albajar P, Cañas E, et al. Diagnosis, management and treatment of chronic Chagas' heart

disease in areas where Trypanosoma cruzi infection is not endemic [in Spanish]. Rev Esp Cardiol. 2007;60(3):285e93.
72. WHO: Soil-transmitted helminth infections. http://www.who.int/mediacentre/factsheets/fs366/en/.
73. Lim JH. Parasitic diseases in the abdomen: imaging findings. Abdom Imaging. 2008;33:130–2.
74. Reeder MM. The radiological and ultrasound evaluation of ascariasis of the gastrointestinal, biliary, and respiratory tracts. Semin Roentgenol. 1998;33:57–78.
75. Choudhuri H, Thappa DM, Kumar RH, et al. Bone changes in leprosy patients with disabilities/deformities (a clinico-radiological correlation). Indian J Lepr. 1999;71:203–15.
76. Ochoa MT, Valderrama L, Ochoa A, et al. Lepromatous and tuberculoid leprosy: clinical presentation and cytokine responses. Int J Dermatol. 1996;35(11):786–90.
77. WHO: Taeniasis/cysticercosis; 2017. http://www.who.int/mediacentre/factsheets/fs376/en/.
78. Kraft R. Cysticercosis: an emerging parasitic disease. Am Fam Physician. 2007;76:91–6.
79. Abdel Razek AA, Watcharakorn A, Castillo M. Parasitic diseases of the central nervous system. Neuroimaging Clin N Am. 2011;21:815–41, viii.
80. Kimura-Hayama ET, Higuera JA, Corona-Cedillo R, et al. Neurocysticercosis: radiologic-pathologic correlation. Radiographics. 2010;30(6):1705–19.
81. WHO: Toxoplasmosis Fact Sheet. http://www.euro.who.int/__data/assets/pdf_file/0011/294599/Factsheet-Toxoplasmosis-en.pdf?ua=1.
82. Lee GT, Antelo F, Mlikotic AA. Cerebral Toxoplasmosis. Radiographics. 2009;29(4):1200–5.
83. Malinger G, Werner H, Rodriguez Leonel JC, et al. Prenatal brain imaging in congenital toxoplasmosis. Prenat Diagn. 2011 Sep;31(9):881–6.
84. WHO: Foodborne trematode infections: Clonorchiasis. http://www.who.int/foodborne_trematode_infections/clonorchiasis/en/.
85. Lim JH. Radiologic findings of clonorchiasis. Am J Roentgenol. 1990;155(5):1001–8.
86. Lim JH, Kim SY, Park CM. Parasitic diseases of the biliary tract. Am J Roentgenol. 2007;188(6):1596–603.
87. Antimicrobe: Entamoeba histolytica (Amebiasis). http://www.antimicrobe.org/new/b137.asp.
88. Araujo Júnior E, Carvalho FH, Tonni G, Werner H. Prenatal imaging findings in fetal Zika virus infection. Curr Opin Obstet Gynecol. 2017;29(2):95–105.
89. Oliveira-Szengnfeld, et al. Congenital brain abnormalities and zika virus: what the radiologist can expect to see prenatally and postnatally. Radiology. 2016;281:1–16.
90. Brasil P, Pereira JP, Moreira ME, et al. Zika virus infection in pregnant women in Rio de Janeiro. N Engl J Med. 2016;375(24):2321–34.
91. Stegmann BJ, Carey JC. TORCH infections: toxoplasmosis, other (syphilis, varicella-zoster, parvovirus B19), rubella, cytomegalovirus and herpes infections. Current Womens Health. 2002;2(4):253–8.